Int. J. Multiphase Flow Vol. 13, No. 4, pp. 443–458, 1987
Printed in Great Britain.

0301-9322/87 $3.00 + 0.00

INSTABILITIES IN SELF-FLUIDIZED BEDS—I

THEORY

D. GREEN and G. M. HOMSY
Department of Chemical Engineering, Stanford University, Stanford, CA 94305, U.S.A.

(*Received* 12 *May* 1986; *in revised form* 24 *December* 1986)

Abstract—The stability of self-fluidized beds is analyzed using the two-fluid equations of fluidization. The base-state profiles consist of a packed region of uniform voidage underlying an expanded, fluidized state. The stability analysis takes into account the communication between the packed and fluidized region, which leads to a set of stability equations very similar to that solved previously by Medlin *et al.* The results indicate that self-fluidized beds are always unstable to spatially periodic circulatory modes. Parametric studies indicate that there is good qualitative and quantitative agreement between theory and the parametric dependencies measured experimentally.

1. INTRODUCTION

In the companion paper (Green & Homsy 1987), the results of an experimental investigation of the instability found for self-fluidization are presented. In this paper, a linear stability analysis of the "two-fluid" equations of motion for self-fluidization is employed to investigate our ideas regarding the mechanism of the instability.

The experimental investigation found that the instability occurred in two stages: a primary instability consisting of a steady, spatially periodic array of spouts and a secondary instability comprised of the temporally periodic growth and expiration of a single large spout. The secondary instability is clearly a non-linear effect and its description is therefore beyond the linear analysis undertaken here.

It is the primary instability, then, that is the subject of this investigation. We have proposed a mechanism by which infinitesimal perturbations to the local void fraction could possibly become unstable. By this mechanism, the preferred spatial wavelength is the result of competing effects; the pressure field in the packed region beneath the plane of minimum fluidization and particle inertia which favor the growth of disturbance at small wavelengths, and the viscous-like resistance to shear of the particle phase which acts to damp disturbances with very short wavelengths.

One objective, then, of this theoretical investigation is to further examine this proposed mechanism to see if it is supported by a set of dynamical equations. Also, prediction of the rate of growth and the wavelength of the primary instability is sought from knowledge of the parameters of the flow and the particles as well as those appearing in the continuum equations. The sensitivity of these characteristics of the instability to the parameters is to be determined, allowing a comparison to be made between the observed characteristics of the primary instability and those predicted by the analysis.

The instability of conventionally fluidized beds has been analyzed by several investigators. Pigford & Baron (1965), Anderson & Jackson (1968) and Homsy *et al.* (1980) solved for temporally growing periodic plane disturbances. All found exponentially growing disturbances for all values of the parameters studied, with plane waves being the preferred mode. Thus the instability modes in conventional fluidization are substantially different from what is observed in self-fluidization.

More closely aligned with the current work are two studies of Jackson and coworkers. In a study of the circulatory instability observed for low aspect ratio beds when the pressure drop across the distributor is small compared to the pressure drop across the bed, Medlin *et al.* (1974) allowed periodic *horizontal* disturbances and solved for the form of the disturbances in the streamwise (vertical) direction. They found temporally growing, spatially periodic modes for sufficiently wide beds when the ratio of support to bed pressure drop was below a certain critical value. In a later study, Medlin & Jackson (1975) extended the previous results, which had assumed the support

pressure drop to be concentrated in a plane, to supports of finite thickness. They found that the stabilizing effect of the distributor pressure drop decreased as the thickness of the distributor increased.

Although not immediately apparent, certain parallels may be drawn between self-fluidization and the system studied in these papers. In both, the flow in a fluidized section is coupled to the flow feeding into it from below—the flow through the distributor in the former case and through the packed section in the case of self-fluidization. Also, the observed instability in both cases has a circulatory nature in 2-D with a horizontally periodic arrangement of cells. The two systems differ in details; however, it is believed that the basic mechanism, allowed by coupling between flow in a fluidized region and that in a packed section, is operative in both cases.

The approach of the current work then is to perform a linear stability analysis of the two-fluid equations, altered so as to include the effect of a spatially uniform steady source. Disturbances that are periodic in the horizontal direction will be sought and the dependence of the stability characteristics on the various parameters will be studied. Insofar as is possible, these predictions will be compared to our experimental observations of the primary instability.

2. FORMULATION

Equations

The equations chosen for this investigation are the so-called "two-fluid" equations, which are a relatively simple set of equations written on both the fluid and the particulate phases of the fluidized system. The phases are viewed as interpenetrating continua, i.e. the system is viewed on a length scale that is large enough that the details of the flow on the scale of individual particles are not resolved, but that is still small relative to the length scales of the apparatus and of the phenomena that are to be analyzed. These equations have been discussed in detail in the literature (Anderson & Jackson 1968; Homsy *et al.* 1980; Jackson 1985). The equations, written for self-fluidization are, from continuity,

fluid

$$\frac{\partial \epsilon}{\partial t} + \nabla \cdot (\epsilon \mathbf{u}) - S = 0 \qquad [1]$$

and

solid

$$\frac{\partial (1-\epsilon)}{\partial t} + \nabla \cdot [(1-\epsilon)\mathbf{v}] = 0; \qquad [2]$$

and from conservation of linear momentum,

fluid

$$\rho_f \left(\frac{\partial \mathbf{u}}{\partial t} + \mathbf{u} \cdot \nabla \mathbf{u} \right) = \nabla \cdot \mathbf{T}_f + \mathbf{I} + \rho_f \mathbf{g} \qquad [3]$$

and

solid

$$\rho_s \left(\frac{\partial \mathbf{v}}{\partial t} + \mathbf{v} \cdot \nabla \mathbf{v} \right) = \nabla \cdot \mathbf{T}_s - \mathbf{I} + \rho_s \mathbf{g}; \qquad [4]$$

where ρ_f and ρ_s are the fluid and solid continuum densities, respectively; ϵ is the local void fraction; and $\mathbf{u}$ and $\mathbf{v}$ are the fluid and solid velocities, respectively. The term involving S in [1] represents the source of fluid within the bed. It is assumed for the purposes of this analysis to be constant both in space and time, which includes the effect of the source in the equations of motion in the simplest possible way. Although this choice limits the generality of the work, it is believed to be justified in this exploratory treatment. The change in mass of the solid phase is neglected, being assumed to be much less than the change in mass of the fluid. $\mathbf{T}_f$ and $\mathbf{T}_s$ are the partial stress tensors

for the fluid and solid phases, respectively, which embody the pressure and viscous effects. Constitutive relations for the partial stress tensors and the interaction force **I** are necessary in order to close this system of equations.

In the spirit of presenting the simplest possible theory which encompasses the mechanics we consider to be important, we neglect any viscous effects in the fluid momentum equation, as well as any virtual mass effects in the interaction force. In addition, we neglect the terms in [3] associated with the inertia of the fluid. Also in keeping with previous analyses, we adopt a pseudo-Newtonian closure for the particle stress. These assumptions lead to the following relations:

$$I_i = -p_f \frac{\partial(1-\epsilon)}{\partial x_i} - \alpha(u_i - v_i), \qquad [5]$$

$$T_{ij,f} = -p_f \epsilon \delta_{ij} \qquad [6]$$

and

$$T_{ij,s} = -p_s(1-\epsilon)\delta_{ij} + \beta d_{kk}\delta_{ij} + 2\eta(d_{ij} - d_{kk}\delta_{ij}), \qquad [7]$$

where

$$d_{ij} = \frac{1}{2}\left(\frac{\partial v_i}{\partial x_j} + \frac{\partial v_j}{\partial x_j}\right). \qquad [8]$$

The notation follows previous work, where p_f and p_s are the fluid and solids pressure, α is a drag coefficient and β and η are the bulk and shear viscosities of the particulate phase, respectively.

Scaling

Figure 1 gives a schematic of the system under consideration. In order to non-dimensionalize the system of equations, the following characteristic dimensions are chosen. The height of the slumped bed, H_0 is chosen as the characteristic length and the inverse of the source strength, $1/S$, as the characteristic time. SH_0 is then the characteristic velocity, and the following dimensionless quantities may be defined:

$$\hat{x}_i = \frac{x_i}{H_0}; \quad \hat{t} = tS; \quad \hat{u}_i = \frac{u_i}{SH_0}; \quad \hat{v}_i = \frac{v_i}{SH_0};$$

and

$$\hat{p}_{f,s} = \frac{p_{s,f}}{\rho_s S^2 H_0^2}.$$

Non-dimensionalizing and substituting the above forms of I_i and T_{ij}, the equations become (dropping the circumflexes)

$$\frac{\partial \epsilon}{\partial t} + \frac{\partial \epsilon u_k}{\partial x_k} - 1 = 0, \qquad [9]$$

$$\frac{\partial(1-\epsilon)}{\partial t} = \frac{\partial(1-\epsilon)v_k}{\partial x_k} = 0, \qquad [10]$$

$$\frac{\partial p_f}{\partial x_i} = -\frac{R}{\mathrm{Re}}\alpha(u_i - v_i) - R\,\mathrm{Fr}\,\delta_{i3} \qquad [11]$$

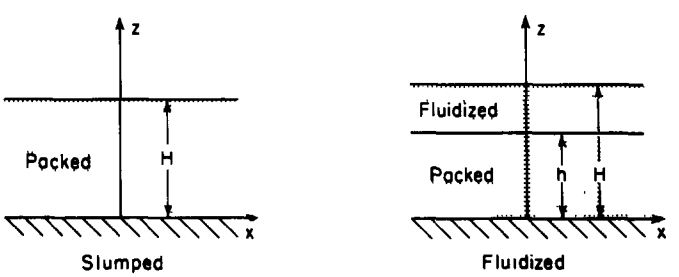

Figure 1. Schematic of a self-fluidized bed.

and

$$(1-\epsilon)\left(\frac{\partial v_i}{\partial t}+v_j\frac{\partial v_i}{\partial x_j}\right)=\frac{R}{\mathrm{Re}}\left\{\frac{\partial}{\partial x_i}\left(\beta\frac{\partial v_k}{\partial x_k}\right)+\frac{\partial}{\partial x_j}\left[\eta\left(\frac{\partial v_i}{\partial x_j}+\frac{\partial v_j}{\partial x_i}-\frac{2}{3}\frac{\partial v_k}{\partial x_k}\delta_{ij}\right)\right]+\alpha(u_i-v_i)\right\}$$

$$-\frac{\partial}{\partial x_i}[(1-\epsilon)(p_s-p_f)]-(1-\epsilon)\,\mathrm{Fr}\,\delta_{i3}. \qquad [12]$$

Neglecting the inertia and viscosity of the fluid leads to Darcy's law [11], for the relationship between the pressure gradient in the fluid phase and the relative velocity. Inclusion of solid-phase inertia and viscous-like resistance to shear produces [12], which is similar in form to a simple compressible momentum equation written for the solid phase. The difference is that terms representing the drag between the phases are included, and the pressure appears as the difference between the solid- and fluid-phase pressures. Here the dimensionless parameters are

$$R=\frac{\rho_f}{\rho_s},\quad \mathrm{Re}=\frac{SH_0^2\rho_f}{\mu_f},\quad \mathrm{Fr}=\frac{g}{S^2H_0}; \qquad [13]$$

and α, β, μ are the *dimensionless* drag coefficient, bulk and shear viscosities, respectively. For details, see Green (1986).

Flow in the packed section and boundary conditions

A fluidized region of finite depth and infinite horizontal extent is considered. Therefore, boundary conditions are required at the upper and lower boundaries of the fluidized layer. For a uniform source, the velocity of the fluid will increase with increasing height in the bed, and since the bed support is impermeable, the fluid velocity must be zero there. Therefore, the velocity will be insufficient to fluidize the bed in a region above the distributor and below a certain level in the bed determined by the strength of the source, refer to figure 1. The fluid flow in the lower part of the bed will be the flow through a packed section which, with our approximations, will be a Darcy flow. Barring velocities at the upper surface of the bed high enough to cause entrainment, the flow in the freeboard region above the bed will simply be the unbounded flow of the clear fluid.

The location at which the bed becomes fluidized will be called the "plane of minimum fluidization," and its dimensionless location denoted by $z=h$. Below this plane, the flow is through a packed section of infinite horizontal extent and constant void fraction. The fluid continuity equation applies in the packed section, but the solid phase is quiescent and the solid-phase continuity equation is identically satisfied. These equations are:

continuity

$$\epsilon_0\frac{\partial u_k}{\partial x_k}-1=0; \qquad [14]$$

and

Darcy's law

$$\frac{\partial p_f}{\partial x_i}=-\frac{R}{\mathrm{Re}}\alpha_0 u_i-R\,\mathrm{Fr}\,\delta_{i3}; \qquad [15]$$

ϵ_0 is the value of the void fraction in the packed section, and $\alpha_0\equiv\alpha(\epsilon_0)$.

Consideration of the conservation of mass and momentum across the surface of minimum fluidization leads to a set of equations linking the flow in the packed and the fluidized layers. The following jump conditions are then imposed across the boundary separating the fluidized from the unfluidized sections of the bed, $\mathbf{n}$ being the unit normal to this boundary:

at $z=h$,

$$[\epsilon\mathbf{u}\cdot\mathbf{n}]=0, \qquad [16]$$

$$[\epsilon p_f]=0, \qquad [17]$$

$$[(1-\epsilon)\mathbf{v}\cdot\mathbf{n}]=0 \qquad [18]$$

and

$$\mathbf{n}\cdot\mathbf{T}^s = \mathbf{0}. \tag{19}$$

Here the square brackets denote the jump in the quantity across the boundary. Consideration of the tangential stress balance of the solid phase at the surface of minimum fluidization is not entirely clear. Two extremes are possible: no slip or no shear stress at the boundary. Medlin *et al.* (1974) found their results for conventionally fluidized systems were not sensitive to the choice of this boundary condition. The zero shear stress condition implied by [19] will be used throughout the present investigation.

Above the fluidized layer in the freeboard region, the fluid flow will be considered inviscid and unbounded. The fluid density is low, so inertial effects are small as well. This places no restriction on the fluid velocities issuing from the upper surface of the fluidized region. The only restriction on the fluid phase will be that the pressure in the freeboard region near the boundary is constant (Medlin *et al.* 1974). Since the upper surface is mobile, rigorous conditions there should include, as usual, the kinematic condition coupling surface deflections to bulk velocities. In this work, we will ignore such deflections and confine ourselves to instability modes which are not *essentially* free surface modes. In the absence of entrainment, the velocity of the solid phase normal to the top surface is therefore zero. Therefore, the following boundary conditions are imposed after considering mass and momentum transfer across the upper boundary:

at $z = H$,

$$[\epsilon p_f] = 0, \tag{20}$$

$$[(1-\epsilon)\mathbf{v}\cdot\mathbf{n}] = 0 \tag{21}$$

and

$$\mathbf{n}\cdot\mathbf{T}^s = \mathbf{0}. \tag{22}$$

These jump conditions [16]–[22] coupled with the solution to the flow beneath the surface of minimum fluidization and the constant-pressure condition in the freeboard region provide the necessary boundary conditions to determine the flow in the fluidized layer.

3. BASE STATE

This set of equations possesses a particularly simple 1-D solution which is analogous to the state of "uniform fluidization" found for conventional fluidization. The solution for uniform fluidization is that the void fraction is homogeneous everywhere in the bed, the fluid velocity is uniform and only in the vertical direction and the solid phase is quiescent. The addition of the source term in the equations for self-fluidization requires the steady state to depend on the vertical coordinate, z. Thus we have, for the base state $\epsilon = \bar{\epsilon}(z)$, $p_f = \bar{p}_f(z)$, $u_i = \bar{u}(z)\delta_{i3}$ and $v_i = 0$. For steady flow and stationary solids, the solids in the fluidized region will be supported by the fluid drag force and the phase pressures will be equal, i.e. $p_s = p_f$. The equations governing the base state are then

$$\frac{\mathrm{d}(\bar{\epsilon}\bar{u})}{\mathrm{d}z} = 1,$$

$$\frac{\mathrm{d}\bar{p}_f}{\mathrm{d}z} = -\frac{R}{\mathrm{Re}}\bar{\alpha}\bar{u} - R\,\mathrm{Fr} \tag{23}$$

and

$$\frac{R}{\mathrm{Re}}\bar{\alpha}\bar{u} - (1-\bar{\epsilon})\,\mathrm{Fr} = 0, \tag{24}$$

where $\bar{\alpha} = \alpha(\bar{\epsilon})$.

This gives three equations in the four unknowns: $\bar{\epsilon}$, $\bar{u}$, $\bar{p}_f$ and $\bar{\alpha}$. Since the drag coefficient, $\bar{\alpha}$, will in general be a function of ϵ, the form of α can be specified by introducing a drag law. The widely used Richardson–Zaki correlation will be employed here (Richardson & Zaki 1954). For the

interstitial velocity, $\bar{u}$, this gives $\bar{u} = u_t \epsilon^{n-1}$ where u_t and n are the usual Richardson–Zaki parameters; note that u_t is made dimensionless with respect to SH_0.

In order to solve this system, boundary conditions must be applied at the plane of minimum fluidization. First, the steady-state solution for the flow in the packed section must be obtained and the plane of minimum fluidization located. The boundary conditions are then obtained by applying the jump conditions [16] and [17] to the steady-state solutions, the other conditions being trivially satisfied.

In the packed section, $z < h$, the steady-state solutions are

$$\bar{u} = \frac{z}{\epsilon_0}, \tag{25}$$

$$\bar{p}_f = -\left(\frac{R\alpha_0}{2\,\mathrm{Re}\,\epsilon_0}\right) z^2 - R\,\mathrm{Fr}\,z + p_{f_0} \tag{26}$$

and

$$\bar{p}_s = \left[\frac{R\alpha_0}{2\,\mathrm{Re}\,(1-\epsilon_0)}\right] z^2 - \mathrm{Fr}\,z + p_{s_0}. \tag{27}$$

The boundary between the fluidized and unfluidized layers will be a plane under steady conditions. It is located in the usual way from the condition that the local fluid velocity balances the net weight of the particles. This results in the following dimensionless height:

$$h = \frac{\mathrm{Fr}\,\mathrm{Re}\,\epsilon_0(1-\epsilon_0)}{R\alpha_0}. \tag{28}$$

The steady-state solutions in the fluidized layer, $h < z < H$, are then

$$\bar{\epsilon} = \left(\frac{z}{u_t}\right)^{\frac{1}{n}}, \tag{29}$$

$$\bar{u} = u_t \left(\frac{z}{u_t}\right)^{\frac{(n-1)}{n}}, \tag{30}$$

$$\bar{\alpha}_3 = \frac{\mathrm{Fr}\,\mathrm{Re}}{u_t R}\left[\left(\frac{z}{u_t}\right)^{\frac{(1-n)}{n}} - \left(\frac{z}{u_t}\right)^{\frac{(2-n)}{n}}\right] \tag{31}$$

and

$$\bar{p}_f = \mathrm{Fr}\left[\left(\frac{n}{n+1}\right)\frac{z^{\frac{(n+1)}{n}}}{u_t^{(1/n)}} - z\right] + p_{f_0} - \frac{R\alpha_0 h^2}{2\,\mathrm{Re}\,\epsilon_0} - \mathrm{Fr}\left[\left(\frac{n}{n+1}\right)\frac{h^{\frac{(n+1)}{n}}}{u_t^{(1/n)}} - h\right]. \tag{32}$$

The upper bed limit, $z = H$, is located by considering the conservation of volume of the solids phase. The total volume of the solids is obtained from the following expression for the slumped bed: $V_{\text{solids}} = (1-\epsilon_0)H_0$. Upon fluidizing, the following holds:

$$V_{\text{solids}} = \int_0^H (1-\epsilon)\,\mathrm{d}z = \int_0^h (1-\epsilon_0)\,\mathrm{d}z + \int_h^H [1-\bar{\epsilon}(z)]\,\mathrm{d}z. \tag{33}$$

Integrating, we obtain the following expression for H:

$$H - \left(\frac{n}{n+1}\right)\left[\frac{H^{\frac{(n+1)}{n}}}{u_t^{(1/n)}}\right] = (1-\epsilon_0)H_0 + \epsilon_0 h - \left(\frac{n}{n+1}\right)\left[\frac{h^{\frac{(n+1)}{n}}}{u_t^{(1/n)}}\right]. \tag{34}$$

The bed is then in an expanded state with $H > H_0$. The fluid velocity and local void fraction increase with height within the bed. Profiles of $\bar{u}$ and $\bar{\epsilon}$ are shown in figure 2 for a typical choice of parameters. Under these conditions, the plane of minimum fluidization is at $z = 0.69$. There is a discontinuity in the slope of the fluid velocity at this height as the bed makes the transition from packed to fluidized behavior, and the void fraction increases in the fluidized section.

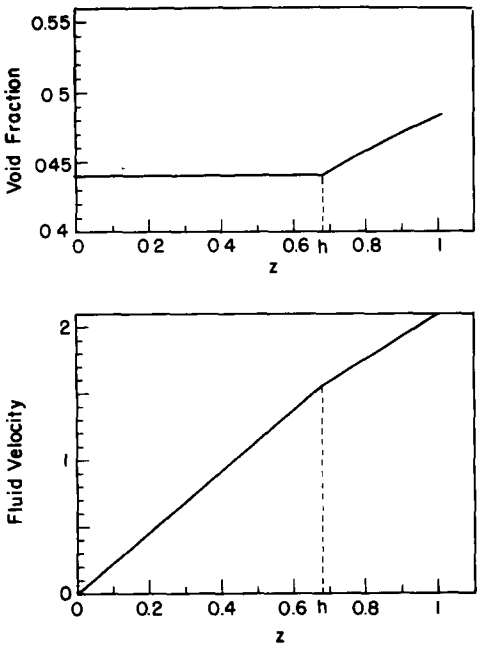

Figure 2. A typical base-state profile.

4. LINEAR STABILITY ANALYSIS

It is well-known that the state of uniform fluidization of conventionally fluidized beds is not observed in practice; instead the flow is characterized by instability. Similarly, it is clear that the flow observed in the self-fluidization experiments is nothing like the steady- or base-state solution predicted by the theory; instead, the flow is likewise dominated by an instability.

The base-state predictions obtained above represent a 1-D solution to the two-fluid equations, whose stability we now examine. This is done by allowing perturbations to the base-state solutions in the usual fashion:

$$\left.\begin{aligned} \epsilon &= \bar{\epsilon} + \epsilon' \\ p_f &= \bar{p}_f + p_f' \\ u_i &= \bar{u}\delta_{i3} + u_i' \\ v_i &= v_i', \end{aligned}\right\} \qquad [35]$$

where the overbar indicates the base-state solutions obtained above. The sum of base-state and perturbation quantities can be substituted into the full set of time-dependent equations [9]–[12]. By assuming that the perturbations to the base state are small, quadratic and high-order terms of the perturbation quantities are neglected. After subtracting the base-state equations, the result is a set of simultaneous linear partial differential equations in the perturbation quantities. The pressure difference between the phases $[p_s - p_f]$ is allowed to be a function of ϵ. Also, as is well-known, $\alpha = \alpha(\epsilon)$. These two parameters are then expanded:

$$(p_s - p_f) = \epsilon' \left.\frac{d(p_s - p_f)}{d\epsilon}\right|_{\bar{\epsilon}} \qquad [36]$$

and

$$a' = \alpha(\bar{\epsilon}) + \epsilon' \left.\frac{d\alpha}{d\epsilon}\right|_{\bar{\epsilon}} = \bar{\alpha} + \epsilon' \left.\frac{d\alpha}{d\epsilon}\right|_{\bar{\epsilon}}. \qquad [37]$$

The resulting equations are linear in the perturbation quantities. They are written here in vector form:

$$\frac{\partial \epsilon'}{\partial t} + \frac{\partial (\bar{u}\epsilon')}{\partial z} + \nabla \cdot (\bar{\epsilon}\mathbf{u}') = 0, \tag{38}$$

$$-\frac{\partial \epsilon'}{\partial t} + \nabla \cdot [(1-\bar{\epsilon})\mathbf{v}'] = 0, \tag{39}$$

$$\nabla p_f' = -\frac{R}{\mathrm{Re}}\left[\bar{\alpha}(\mathbf{u}' - \mathbf{v}') + \bar{u}\frac{\mathrm{d}\alpha}{\mathrm{d}\epsilon}\bigg|_{\bar{\epsilon}} \epsilon' \mathbf{k}\right] \tag{40}$$

and

$$(1-\bar{\epsilon})\frac{\partial \mathbf{v}'}{\partial t} = \frac{R}{\mathrm{Re}}\left\{\beta\nabla(\nabla\cdot\mathbf{v}') + \eta[\nabla^2\mathbf{v}' + \tfrac{1}{3}\nabla(\nabla\cdot\mathbf{v}')] + \bar{\alpha}(\mathbf{u}'-\mathbf{v}') + \bar{u}\frac{\mathrm{d}\alpha}{\mathrm{d}\epsilon}\bigg|_{\bar{\epsilon}}\epsilon'\mathbf{k}\right\} - \nabla\left[(1-\bar{\epsilon})\frac{\mathrm{d}(p_s - p_f)}{\mathrm{d}\epsilon}\bigg|_{\bar{\epsilon}}\epsilon'\right] + \mathrm{Fr}\,\epsilon'\mathbf{k}. \tag{41}$$

Because of their linearity and the fact that the coefficients are independent of time and the horizontal or cross-stream coordinates, these equations admit exponential solutions in those dimensions. Considering solutions in two spatial dimensions, x and z (figure 1), and expressing the variables in terms of their normal modes in t and x, we have

$$\begin{vmatrix} \epsilon' \\ p_f' \\ u_i' \\ v_i' \end{vmatrix} = \begin{vmatrix} E(z) \\ P(z) \\ U_i(z) \\ V_i(z) \end{vmatrix} e^{(ikx+\sigma t)}. \tag{42}$$

Substituting into [38]–[41] yields a set of linear ordinary differential equations in z for $E(z)$ etc, in which the eigenvalue is the growth constant, σ, introduced above; k is the wavenumber of the disturbances in the x or horizontal direction. The ordinary differential equations are as follows:

$$\left(\alpha + \frac{\mathrm{d}\bar{u}}{\mathrm{d}z}\right)E + \bar{u}\frac{\mathrm{d}E}{\mathrm{d}z} + \bar{\epsilon}\left(ikU_x + \frac{\mathrm{d}U_z}{\mathrm{d}z}\right) + \frac{\mathrm{d}\bar{\epsilon}}{\mathrm{d}z} = 0, \tag{43}$$

$$-\sigma E + (1-\bar{\epsilon})\left(ikV_x + \frac{\mathrm{d}V_z}{\mathrm{d}z}\right) - \frac{\mathrm{d}\bar{\epsilon}}{\mathrm{d}z}V_z = 0, \tag{44}$$

$$ikP = -\frac{R}{\mathrm{Re}}\bar{\alpha}(U_x - V_x), \tag{45}$$

$$\frac{\mathrm{d}P}{\mathrm{d}z} = -\frac{R}{\mathrm{Re}}\left[\bar{\alpha}(U_z - V_z) + \frac{\mathrm{d}\alpha}{\mathrm{d}\epsilon}\bigg|_{\bar{\epsilon}}\bar{u}E\right], \tag{46}$$

$$(1-\bar{\epsilon})\sigma V_x = \frac{R}{\mathrm{Re}}\left[\left(\beta + \frac{\eta}{3}\right)\left(ik\frac{\mathrm{d}V_z}{\mathrm{d}z} - k^2V_x\right) + \eta\left(\frac{\mathrm{d}^2V_x}{\mathrm{d}z^2} - k^2V_x\right) + \bar{\alpha}(U_x - V_x)\right] - (1-\bar{\epsilon})\frac{\mathrm{d}(p_s-p_f)}{\mathrm{d}\epsilon}\bigg|_{\bar{\epsilon}} ikE \tag{47}$$

and

$$(1-\epsilon)\sigma V_z = \frac{R}{\mathrm{Re}}\left\{\left(\beta + \frac{\eta}{3}\right)\left(ik\frac{\mathrm{d}V_x}{\mathrm{d}z} + \frac{\mathrm{d}^2V_z}{\mathrm{d}z^2}\right) + \eta\left(\frac{\mathrm{d}^2V_z}{\mathrm{d}z^2} - k^2V_z\right) + \bar{\alpha}(U_z - V_z) + \frac{\mathrm{d}\alpha}{\mathrm{d}\epsilon}\bigg|_{\bar{\epsilon}}uE\right\} - \frac{\mathrm{d}}{\mathrm{d}z}\left[(1-\epsilon)\frac{\mathrm{d}(p_s-p_f)}{\mathrm{d}\epsilon}\bigg|_{\bar{\epsilon}}\right]\frac{\mathrm{d}E}{\mathrm{d}z} + \mathrm{Fr}\,E. \tag{48}$$

The conditions coupling the perturbation quantities in the fluidized layer with those in the packed and clear fluid regions are written below. Both the surface of minimum fluidization and the upper bed surface are assumed to remain planar in the presence of the disturbances. Written in terms of the variables of the normal mode analysis, the boundary conditions [16]–[22] become

$$[V_z]_{h+} = 0, \tag{49}$$

$$[\bar{u}E + \bar{\epsilon}U_z]_{h+} = [\epsilon_0 U_z]_{h-}, \tag{50}$$

$$[\bar{\epsilon}P + \bar{p}_f E]_{h+} = [\epsilon_0 P]_{h-}, \tag{51}$$

$$\left[\frac{dV_x}{dz}\right]_{h+} = 0, \tag{52}$$

$$[P]_{H-} = 0, \tag{53}$$

$$[V_z]_{H-} = 0 \tag{54}$$

and

$$\left[\frac{dV_x}{dz}\right]_{H-} = 0. \tag{55}$$

These equations are coupled, through [50] and [51], to the fluctuations in the packed section. The latter may be treated analytically as follows. Allowing perturbations to the fluid velocity and pressure of the flow beneath the plane of minimum fluidization, but keeping the void fraction fixed and solids stationary since this is a packed section, the linearized equations are

$$\frac{\partial u_k'}{\partial x_k} = 0 \tag{56}$$

and

$$\frac{\partial p_f'}{\partial x_i} = -\frac{R}{\mathrm{Re}}\alpha_0 u_i'; \tag{57}$$

or, in terms of normal modes,

$$ikU_x + \frac{dU_z}{dz} = 0, \tag{58}$$

$$ikP = -\frac{R}{\mathrm{Re}}\alpha_0 U_x \tag{59}$$

and

$$\frac{dP}{dz} = -\frac{R}{\mathrm{Re}}\alpha_0 U_z. \tag{60}$$

Solving this along with the following boundary conditions at the bed support, $z = 0$:

$$U_z(z = 0) = 0 \tag{61}$$

and

$$P(z = 0) = P_0; \tag{62}$$

we find

$$P = P_0 \cosh(kz) \tag{63}$$

and

$$U_z = -\frac{\mathrm{Re}\, kP_0}{R\alpha_0}\sinh(kz).$$

Substituting into the boundary conditions [49]–[52]:

$$V_z = 0, \tag{64}$$

$$\bar{u}E + \bar{\epsilon}U_z = -\frac{\epsilon_0 \mathrm{Re}\, kP_0}{R\alpha_0}\sinh(kh), \tag{65}$$

$$\bar{\epsilon}P + \bar{p}E = \epsilon_0 P_0 \cosh(kh) \tag{66}$$

and

$$\frac{\mathrm{d}V_x}{\mathrm{d}z} = 0. \tag{67}$$

Six boundary conditions are necessary to determine the solution to the system. These four conditions along with [53]–[55] total seven. However, the magnitude of P_0, which couples the flow in the packed section to that in the fluidized region is also unknown, thus resulting in seven homogeneous conditions.

The coefficients of the set of ordinary differential equations are not constant due to the z dependence of the base state. This fact precludes a direct solution; either numerical integration must be used or further simplification must be implemented.

An attempt was made at a numerical solution using a shooting method, but for relevant choices of the parameters, the system turned out to be very stiff. The solution evidently contains exponentially growing components on very different length scales. A second-order accurate implicit integration scheme was used, but execution was very costly. Solving the set of seven complex simultaneous difference equations once every step of the integration, coupled with the small step size necessitated by the stiffness of the problem, was very time consuming. Consequently, only an extremely limited range of parameters could be explored using this technique. In particular, only a shallow fluidized layer was analyzed since this meant the integration could be carried out over a very small depth.

Therefore, in order to explore a reasonable range of parameters, a further simplification was made. By assuming that the change in the base-state variables is small over the depth of the fluidized layer, the variable coefficients in the linear stability equations can be approximated by constants, with the result that the equations can be solved directly. Of course, this approximation is better for values of the source strength close to that necessary to minimally fluidize the system because the height of the fluidized layer will be small and the change in the base state over that range will also be small. Additionally, by visual observation of the experiments, no great expansion of the fluidized region occurred. The depth of the region seemed to remain modest even at high source strengths as most of the fluid channeled into the spouting structures of the instability and not into an expanded emulsion phase. It is thus believed that the assumption of small change in the base state over the height of the fluidized region is reasonable and should give qualitatively correct results, particularly for small fluidized heights.

The equations are then equivalent in form to those derived by Medlin *et al.* (1974). Following their lead, much algebraic manipulation leads to two simultaneous equations in E and V_z that can be solved directly. The details of this manipulation are identical to those given at length by Medlin *et al.* (1974), and will not be repeated here. Suffice to say that we solve the constant-coefficient version of [43]–[48] in terms of sums of exponentials, and apply the boundary conditions to obtain a determinamental equation. Iteration of the estimates for the growth constant, σ, is then performed until a zero of the determinant is obtained. The process is repeated for different wavenumbers, thus determining the dispersion relation; this was done interactively using a small IBM-PC-XT with 80 bit internal arithmetic. We refer the interested reader to Green (1986) for these and other details.

5. RESULTS

The parameters that govern the stability of the system derived above are: Re and Fr, the Reynolds and Froude numbers based on the slumped height of the bed; R, the density ratio; u_t and n, parameters of the Richardson–Zaki drag relation; β and η, rheological material constants of the particulate phase; and $[\mathrm{d}(p_s - p_f)/\mathrm{d}\epsilon]_\epsilon$, the derivative of the phase-pressure difference

evaluated at the base-state voidage. Of the above, both Re and Fr depend on the source strength, S. The Galileo number, $\mathrm{Re}^2\mathrm{Fr} = \rho_f H_0^3/\mu_f^2$, however, depends only on fluid and particle properties. Therefore, if the problem is recast treating Re and Ga as the independent dynamic parameters rather than Re and Fr, the source strength dependence is captured in a single parameter, Re. Ga and the other parameters are functions only of the fluid and particle properties.

In addition to these dynamic parameters, several material functions must also be specified. Correlations are available for u_t, the terminal velocity of a single particle and n, the Richardson–Zaki exponent. For this analysis, u_t was chosen to match the experimentally observed minimum fluidizing velocity for each particle size considered and n was determined from the correlations of Richardson & Zaki (1954); β and η, the bulk and shear viscosities of the particulate phases respectively, are less well-documented. Viscometric data for fluidized beds are of dubious value due to the poorly understood boundary conditions at the surface of any device immersed in the bed to measure its viscosity. Inferences of these viscous parameters from non-invasive techniques, although less accurate, are more likely to represent intrinsic values. Using measurements of the included angle of spherical cap bubbles in fluidized beds. Grace (1970) inferred values of η from 4 to 13 P. This is the same order of magnitude that has been reported for this quantity elsewhere in the literature (Murray 1967; Hetzler & William 1969). Homsy *et al.* (1980), in a comparison of the predictions of a linear stability analysis with observations of the propagation of planar voidage waves in a liquid fluidized bed, found values of $[\beta + (4/3)\eta]$ to be in the order of 10–100 P. It then seems reasonable that β and η are of the same order of magnitude, but it is impossible to be more precise with the data that are currently available. Little information is available for the derivative of the phase-pressure difference with respect to ϵ, as well. Some investigators have taken it to be equal to zero for gas fluidized beds (Medlin *et al.* 1974). Homsy *et al.* (1980) found values in the order of $-90\ \mathrm{dyne/cm^2}$ for liquid fluidized beds.

In the self-fluidization experiments discussed previously, the particle density, ρ_s, and the fluid viscosity, μ_f, were fixed; u_t and n are determined by the choice of the particle diameter. This then means that there are still 6 available degrees of freedom. These are specified by choosing the following dimensional values: the fluid density, static height, source strength, bulk and shear viscosities and the derivative of the pressure difference.

Because of the difficulties involved in attempting to model a system with so many poorly specified variables, the following standard choices of the parameters were made and each parameter was then varied individually in order to determine its effect on the solution:

standard parameter values

$$\rho_f = 3 \times 10^{-6}\ \mathrm{g/cm^3}$$

$$H_0 = 7.0\ \mathrm{cm}$$

$$d_p = 463\ \mu\mathrm{m}$$

$$S = 9.05\ \mathrm{s^{-1}}$$

$$\beta = \eta = 10\ \mathrm{P}$$

$$\left[\frac{\mathrm{d}(p_s - p_f)}{\mathrm{d}\epsilon}\right] = 0$$

$$\epsilon_0 = 0.44.$$

For each particular combination of the parameters, a relation between the growth constant, σ, and the wavenumber, k, exists. We have chosen to present these results in dimensional as opposed to dimensionless form, since our interest is in comparison with a specific set of experiments. Figure 3 shows the dispersion relation for the standard set of parameters, indicating a clear maximum, and the existence of a preferred wavelength for the instability, echoing the preferred wavelength observed for the disturbances in the experimental study.

Parameter studies

The fluid density was changed from 10^{-5} to $3 \times 10^{-6}\ \mathrm{g/cm^3}$, roughly equal to the range it varied over during a typical experiment. As expected, no effect on the dispersion relation was observed for these low densities.

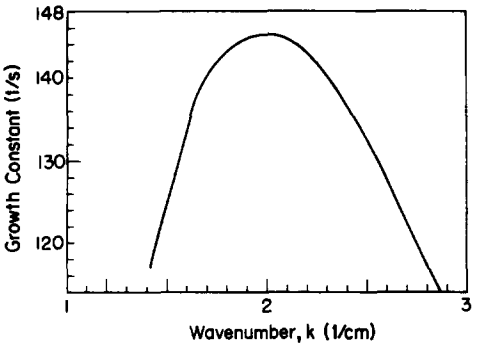

Figure 3. Dispersion relation for the base case.

The source strength was varied over a range of 9.0–16.3 s^{-1} for the 463 μm particles. This corresponds to a range of locations of the plane of minimum fluidization (normalized with the slumped height) of from 0.90 to 0.5. The effect of increasing the source strength is to decrease slightly the most dangerous wavenumber of the instability, as shown in figure 4. The effect is most pronounced for the smaller source strengths, here shown as the $h = 0.90$ to $h = 0.80$ curves. Initially, there is a decrease in the maximum growth constant as the source strength is increased; then, as the source strength is increased above approx. 10.2 s^{-1}, there is a modest increase in the maximum growth constant. Thus, we can conclude that the preferred wavelength is relatively insensitive to the source strength.

The results of varying the particle diameter are shown in figure 5. In this case, the source strengths for each particle size were chosen to yield a constant fluidized depth; this also corresponds to an equal normalized volumetric flow rate, Q/Q_{min}, for each particle size range. As we see, the most dangerous wavenumber was predicted to decrease and the growth constant to increase with increasing particle diameter under these conditions.

Investigating the dependence of the instability on the viscous parameters, β and η were first varied in tandem, i.e. β was set equal to η, and the combination was varied. These results are shown in figure 6. As expected, there is a decrease in the growth constant as well as a decrease in the wavenumber as the values of these viscous parameters are increased. While there is a definite dependence on β and η, the most dangerous wavenumber is not overly sensitive to the values of the viscous parameters. For a variation of β and η of two orders of magnitude, a shift in wavenumber of approx. 50% is predicted. Over the same range of β and η, the growth constant changes approx. 300%, so the stabilizing effect of increasing the viscosity is more substantial than its effect on the preferred wavenumber.

In an effort to further investigate the dependence of the solution on the viscous parameters, the bulk and shear viscosities were varied individually. Little qualitative difference from the results in

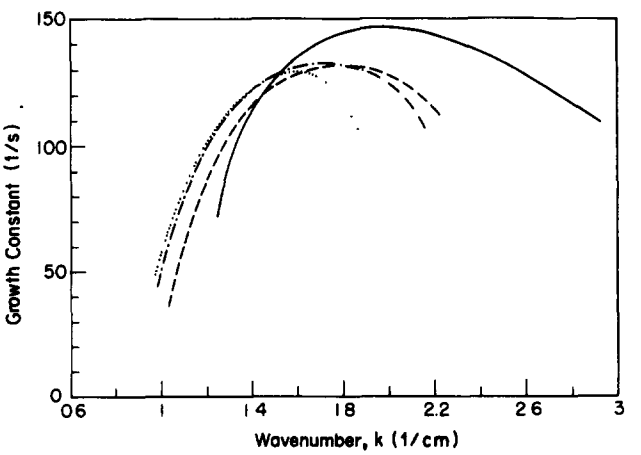

Figure 4. Dispersion relation—effect of source strength: ——, $h = 0.9$; – – –, $h = 0.8$; —·—, $h = 0.7$; ····, $h = 0.5$.

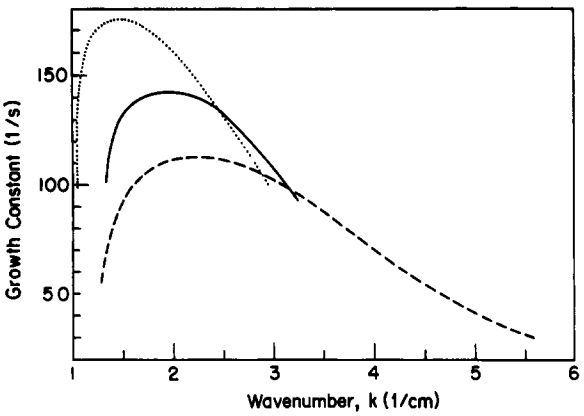

Figure 5. Dispersion relation—effect of particle size: ---, $d_p = 326\ \mu$m; ——, $d_p = 463\ \mu$m; · · · ·, $d_p = 655\ \mu$m.

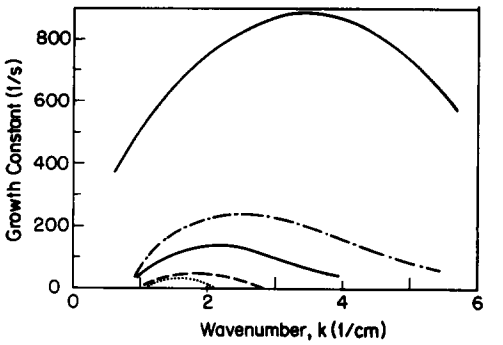

Figure 6. Dispersion relation—effect of rheological parameters $\beta = \eta$. From top to bottom: —— $\eta = 1$ P; —·—, $\eta = 5$ P; ——, $\eta = 10$ P; ---, $\eta = 50$ P; · · · ·, $\eta = 100$ P.

figure 6 was observed for the variation with each of these parameters; for details see Green (1986). Next, the variation of the predictions with the slumped height, H_0, was investigated. The source strength necessary to minimally fluidize the system is a function of the slumped height, so two schemes were used to investigate the dependence of the dispersion relation on H_0.

First, H_0 was varied while the source strength, S, was correspondingly varied in order to maintain $h = 0.90$. This results in a constant value of $Q/Q_{min} = 1.11$. H_0 was varied from 1.0 to 35 cm. Beyond 35 cm, we encountered severe scaling problems in the numerical solution of the determinamental equation and no results for larger values of the slumped height were obtained. Figure 7a shows a general decrease in the wavenumber with increasing H_0 although, as expected, the change is more pronounced for smaller values of H_0. Above about $H_0 = 7$ cm, the shift in the most dangerous wavenumber becomes quite small, although the growth rate continues to increase. Thus we see as expected that for relatively deep beds, the preferred wavelength becomes insensitive to the depth.

The second comparison of results for variation in H_0, was carried out by keeping the dimensional height of the fluidized layer constant at 1.0 cm. Under these conditions, there is a monotonic decrease in the most dangerous wavenumber with H_0 (figure 7b). The growth constant is predicted to increase with increasing H_0 over a range of $H_0 = 4$ to 16 cm.

Three values of the pressure derivative, $[d(p_s - p_f)/d\epsilon]$, were examined. These are 0, -45 and -90 dyne/cm^2, the last being the value that Homsy *et al.* (1980) found gave good agreement between their linear stability predictions and experimental data for liquid fluidized beds. As the pressure derivative becomes increasingly negative, the maximum growth constant decreases and there is a slight decrease in the wavenumber, but the changes are slight; see Green (1986).

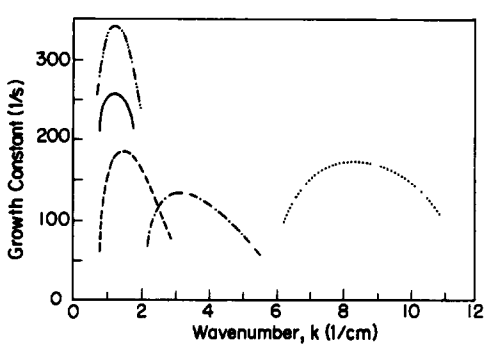

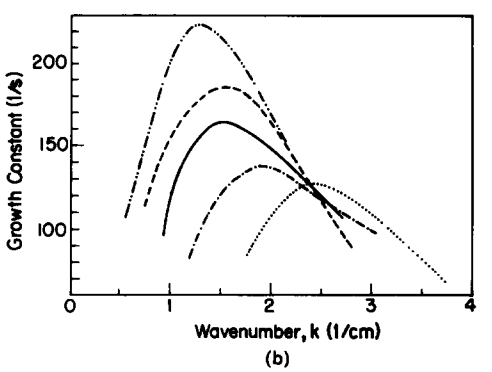

Figure 7. Dispersion relation—effect of slumped height. (a) Dimensionless height of the plane of minimum fluidization held fixed at $h = 0.9$; effect of dimensional slumped height: · · · ·, $H_0 = 1$ cm; —·—, $H_0 = 4$ cm; ---, $H_0 = 7$ cm; ——, $H_0 = 13$ cm; —··—, $H_0 = 20$ cm. (b) Dimensional height of the fluidized region held fixed at $H - h = 1.0$ cm; effect of dimensional slumped height: · · · ·, $H_0 = 4$ cm; —·—, $H_0 = 7$ cm; ——, $H_0 = 10$ cm; ---, $H_0 = 13$ cm; —· ·—, $H_0 = 16$ cm.

In the following section, the results of these parameter studies are discussed and insofar as is possible, compared with the trends observed in the experiments.

6. DISCUSSION

The form of the steady-state solution to the two-fluid equations was found to depend upon z, the vertical coordinate. The fluid velocity increased with z, as expected. This increase in fluid velocity causes further bed expansion, so the void fraction is also found to increase with z. The fluid pressure can be broken down into a constant, a term varying linearly with z corresponding to the hydrostatic contribution and a term increasing non-linearly with z which is due to the varying permeability of the fluidized layer as ϵ varies non-linearly with z.

The position of the plane of minimum fluidization is predicted by setting the drag equal to the weight of the particles at minimum fluidizing conditions. This force balance gives an expression for the height of this plane which decreases with increasing source strength as expected.

A mechanism for the growth of the instability is proposed in the accompanying paper (Green & Homsy 1987). It is postulated that the preferred spatial frequency of the initial instability is the result of the competing effects of particle inertia and the fluid-phase pressure field, favoring the growth of disturbances at short wavelengths, and viscous dissipation in the solids phase damping growth at short wavelengths. The equations used in this study to model the growth of the instability at small amplitudes include these effects. Instability is predicted by these equations with the relation between growth constant and wavenumber of the instability exhibiting a maximum. The wavenumber at which the maximum growth constant occurs corresponds to the existence of an observed preferred wavelength for the instability. The prediction of a maximum in the growth constant/wavenumber curve is strong evidence supporting the validity of the proposed mechanism.

For the entire range of parameters studied, the maximum growth constant obtained was always positive. This indicates that for values of the parameters in the ranges studied, there are always growing modes of the instability for source strengths greater than that necessary to minimally fluidize the system. This finding is in accord with experimental observations.

A limitation of these results arises from the assumption that the base-state velocity and void fraction vary only slightly over the height of the fluidized layer and can be treated as constant. This limits the validity of the results reported here to relatively small fluidized heights and consequently relatively modest source strengths. The fluidized height, however, must be large enough to satisfy the continuum assumption. For this reason, no results are reported for $h > 0.9$.

As discussed above, the characteristics of the instability are governed by the parameters Re, Ga, R, β, η, $[\mathrm{d}(p_s - p_f)/\mathrm{d}\epsilon]$, u_t and n. Fixing p_s and μ_f, and using established drag relations, the effect of varying the following six dimensional parameters was studied: ρ_f, S, d_p, β, η, H_0 and $[\mathrm{d}(p_s - p_f)/\mathrm{d}\epsilon]$.

Values of ρ_f of 10^{-5} and 3×10^{-6} were found to predict the same characteristics of the instability. This is to be expected, since $R \ll 1$ for both choices and the inertia of the fluid can safely be neglected.

At moderate to large source strengths, the growth constant increases with the source strength—the greater fluid flow at higher source strengths accelerating the development and hence the growth rate of the instability. The wavenumber corresponding to the maximum growth constant was found to decrease with increasing S. The effect is largest for small fluidized heights and only modest for $h < 0.7$. The experimental data of the wavelength of the primary instability as a function of $Q/Q_{\min}$, i.e normalized source strength (see Green & Homsy 1987, figures 4–6), suggest that the wavelength increases weakly with increasing source strength. The prediction of the linear stability analysis also has a weak increase of the wavelength with the source strength.

Theoretical predictions were made for the three particle diameters used in the experiments. At source strengths giving a constant location of the plane of minimum fluidization, $h = 0.90$, the maximum growth constant was found to increase with increasing d_p; therefore, at fixed h, the larger particles are less stable than smaller ones. The only place were d_p appears in the problem is in the drag law. The minimum fluidizing velocity is a function of d_p and since u_t and n were determined by matching the minimum fluidizing velocity, they also depend on d_p. The average void fraction in the fluidized layer was found to be virtually identical for all three particle diameters. The decrease

in the instability is due then to the increased permeability of the packed section that is predicted for the larger particles. The most dangerous wavenumber is found to decrease with increasing d_p, predicting longer wavelengths with larger particles. This agrees with the experimental observations (Green & Homsy 1987, table 3). The decreased permeability in the packed section partially relaxes the fluid-pressure field effect that favors the growth of disturbances at short wavelengths. Since the viscous dissipation in the fluidized layer is unaffected by the choice of particle diameter, the wavelength shifts to higher values as the particle diameter is increased.

The predicted maximum growth constant and the most dangerous wavenumber decrease with increasing values of the rheological parameters, β and η. The decrease in wavenumber is caused by increased damping of short wavelengths and the consequent shift to longer preferred wavelengths as the viscous parameter is increased.

Upon varying the slumped height while keeping the ratio of Q/Q_{min} $(=S/S_{min})$ constant, little effect on the wavelength was observed for values of $H_0 \gtrsim 7$ cm. Since most of the experiments were performed at values of $H_0 \approx 10$ cm, this accounts nicely for the lack of variation with slumped height that was observed in the experiments.

Increasing H_0 while keeping the dimensional height of the fluidized layer constant resulted in a monotonic decrease in the most dangerous wavenumber and an increase in the growth constant. This means that the wavelength *does not* scale on the dimensional height of the fluidized layer, but depends upon the slumped height when the source strength is adjusted to keep the fluidized height constant. In general, increasing the slumped height tends to decrease the stability of the system. The effect of the flow in the packed layer is then very important in determining both the maximum growth constant and the most dangerous wavenumber of the instability.

Making a quantitative comparison between the predictions of the linear stability analysis and the experiments is somewhat difficult because there are too many unspecified parameters. β, η and the pressure-difference derivative all drive the predicted wavelength in the same direction and not enough information is available to specify any of the three independently with any degree of certainty. However, some comparisons can be made. As noted above, the trend of the predicted wavelengths agrees with the experimentally observed wavelength of the primary instability with source strength, and particle diameter. The insensitivity of the wavelength to slumped height for slumped height in the range used in the experiments is also predicted. In order to estimate the magnitude of the viscous parameters necessary to predict wavelengths in the range observed experimentally, β was taken equal to η and $[\mathrm{d}(p_s - p_f)/\mathrm{d}\epsilon]_\epsilon$ was set equal to zero. It was found that $\beta = \eta \approx 1$ P predicts wavelengths in the range of those observed. This represents values for these parameters that are in the low part of the range of those reported elsewhere (Grace 1970; Homsy *et al.* 1980). β and η are thought to decrease strongly with increasing void fraction and the minimum value of ϵ used in this analysis was the slumped bed value, $\epsilon_0 = 0.44$. This value is slightly higher than that of many of the systems studied previously. Homsy *et al.* (1980) reported generally lower values of $[\beta + (4/3)\eta]$ for systems with higher values of the slumped void fraction; also, they found $[\beta + (4/3)\eta]$ decreased as the bed expanded. This evidence supports values of these viscous parameters in the range of 1 P for this particular system.

Acknowledgements—We wish to acknowledge the U.S. Department of Energy and the Multiphase Processing Program of the NSF for support of this work.

REFERENCES

ANDERSON, T. B. & JACKSON, R. 1968 Fluid mechanical description of fluidized beds. *Ind. Engng Chem. Fundam.* **7**, 12–21.

GRACE, J. R. 1970 The viscosity of fluidized beds. *Can. J. chem. Engng* **48**, 30–33.

GREEN, D. 1986 Instability in self-fluidization. Ph.D. Thesis, Stanford Univ., Stanford, Calif.

GREEN, D. & HOMSY, G. M. 1987 Instabilities in self-fluidized beds—II. Experiments. *Int. J. Multiphase Flow* **13**, 459–475.

HETZLER, R. & WILLIAM, M. C. 1969 Fluidized bed viscosity and expansion, correlated with a glass-forming liquid model. *Ind. Engng Chem. Fundam.* **8**, 668–677.

HOMSY, G. M., EL-KAISSY, M. M. & DIDWANIA, A. 1980 Instability waves and the origin of bubbles in fluidized beds—II. *Int. J. Multiphase Flow* **6**, 305–318.

JACKSON, R. 1985 Hydrodynamic stability of fluid–particle systems. In *Fluidization* (Edited by DAVIDSON, J. *et al.*). Academic Press, New York.

MEDLIN, J. & JACKSON, R. 1975 Fluid mechanical description of fluidized beds. The effect of distributor thickness on convective instabilitites. *Ind. Engng Chem. Fundam.* **14**, 315–321.

MEDLIN, J., WONG, H. & JACKSON, R. 1974 Fluid mechanical description of fluidized beds. Convective instabilities in bounded beds. *Ind. Engng Chem. Fundam.* **13**, 247–259.

MURRAY, J. D. 1967 On the viscosity of a fluidized system. *Rheol. Acta* **6**, 27–30.

PIGFORD, R. L. & BARON, T. 1965 Hydrodynamic stability of a fluidized bed. *Ind. Engng Chem. Fundam.* **1**, 81–87.

RICHARDSON, J. F. & ZAKI, W. N. 1954 Sedimentation and fluidization: Part I. *Trans. Instn chem. Engrs* **1**, 81–87.